Magnetic Ordering and the Fluorescence of Concentrated Mn Systems*

W. W. Holloway, Jr., E. W. Prohofsky, and M. Kestigian
Sperry Rand Research Center, Sudbury, Massachusetts
(Received 15 March 1965)

The wavelength, lifetime, and relative intensity of the fluorescences of crystal samples of MnF_2 and the alkali manganese trifluorides have been measured as a function of temperature above 21°K. In the vicinity of the Néel temperature, small changes in the fluorescent properties are observed in all samples. At approximately one-half the Néel temperature, larger and more strongly temperature-dependent changes are observed in the fluorescence of these materials. All the salts investigated showed Stokes shifts in their fluorescence spectra. It is believed that the magnetic ordering alters the Stokes shift through the magnetoelastic effect, causing the fluorescent changes observed near the Néel temperature. The low-temperature changes are believed to be caused by the same mechanism when the excited Mn^{2+} ion becomes aligned with respect to the surrounding lattice. The temperature at which this occurs is a measure of the exchange energy for the excited-ion electron configuration. The strong temperature dependence is attributed to a coupling of the lattice distortion with the magnetic interaction of the excited Mn^{2+} ion. This coupling changes the energy of the magnetic virtual local mode centered about the excited ion and causes rapid condensation of the local mode.

INTRODUCTION

RECENTLY, small changes in the fluorescence properties (i.e., wavelength, relative intensity, and time constant) of MnF_2 were described.[1] These changes occur just below, and are apparently related to, the antiferromagnetic ordering at the Néel temperature.

In an earlier communication,[2] striking changes in the fluorescence of MnF_2 and $KMnF_3$ at a much lower temperature were reported. These changes were not observed in the fluorescence of dilute Mn^{2+} systems, and were not directly related to other physical properties, such as crystal-structure changes or the crystal magnetic ordering temperatures.

In this paper, we report additional measurements of the wavelength of the fluorescence, the lifetime, and the relative intensity of the Mn^{2+} fluorescence as a function of temperature for crystal samples of MnF_2 and of the alkali manganese trifluorides (except for $LiMnF_3$). The fluorescences of all samples show temperature-dependent changes.

At least two regions of fluorescence alteration have been observed. The first and smaller temperature-dependent change occurs just below the Néel temperature, and has, therefore, been attributed to the magnetic ordering. We believe that this ordering alters the Stokes shift of the fluorescence through a magnetoelastic effect.

The second class of fluorescent changes occurs at roughly one-half the Néel temperature (hereafter referred to as T_H). The energy change is large compared to the ordering interaction strength, and the temperature dependence is very strong. There appears to be no correlation to other physical properties such as crystal-structure changes. We believe that these observations may be explained on the basis of an alignment of the excited Mn^{2+} ion with respect to the already-ordered ground state. The strong temperature dependence of the excited-state ordering can be explained by a condensation mechanism for local magnetic modes.[3,4] The local mode is centered about the excited Mn^{2+} ion, which has a spin defect in the magnetic lattice. The magnetic alignment of the ion is determined by the thermal activation of the local mode.

EXPERIMENTAL

The fluoride crystals used in these experiments were grown by the horizontal Bridgman technique in an HF atmosphere. Crystal samples of good optical quality were obtained for MnF_2 and all the alkali manganese trifluorides (except for $LiMnF_3$ which we were unable to prepare). Samples of MnF_2, $KMnF_3$, and $RbMnF_3$ were typically $5\times10\times20$ mm and were essentially fracture free. $CsMnF_3$ and $NaMnF_3$ were considerably smaller and contained numerous fractures.

The observations were performed using a Perkin–Elmer type 112-C spectrometer. Samples were mounted with a calorimeter adhesive on a copper post in a metal Dewar provided with windows for optical access. For experimental runs where sizeable samples (i.e., MnF_2, $RbMnF_3$, and $KMnF_3$) were prepared, separate thermocouples monitored the temperatures of both the post and the sample. The difference was at most 4°K at the lower temperatures. For other samples, only the post temperature could be obtained, and the crystal fractures may have contributed to error in the temperature measurement.

A commercial ultraviolet (uv) source (at 3660 Å) provided the excitation for wavelength and intensity meas-

* This work, supported by the U. S. Office of Naval Research Contract NOnr 4127(00), is part of Project DEFENDER under the joint sponsorship of the Advanced Research Projects Agency, the Office of Naval Research and the Department of Defense.

[1] W. W. Holloway, Jr., and M. Kestigian, Phys. Rev. Letters **13**, 235 (1964).

[2] W. W. Holloway, Jr., M. Kestigian, R. Newman, and E. W. Prohofsky, Phys. Rev. Letters **11**, 82 (1963).

[3] E. W. Prohofsky, W. W. Holloway, Jr., and M. Kestigian, J. Appl. Phys. Suppl. **36**, 1041 (1965).

[4] E. W. Prohofsky, Phys. Rev. Letters **14**, 302 (1965).

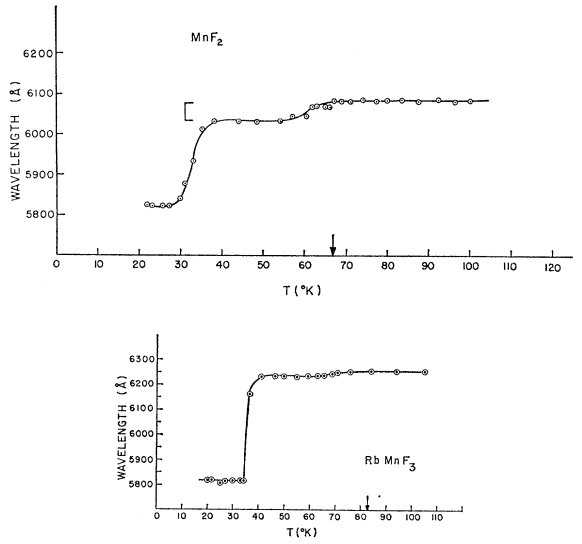

FIG. 1. The maximum wavelength of the fluorescence profiles of MnF_2 and $RbMnF_3$ as a function of temperature. The Néel temperatures are indicated by arrows.

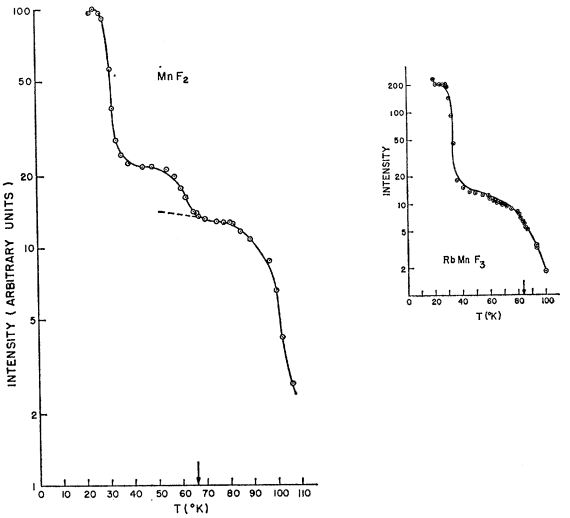

FIG. 2. The relative intensity of the fluorescence profiles of MnF_2 and $RbMnF_3$ as a function of temperature. The Néel temperatures are indicated by arrows.

urements. However, the fluorescence of these crystals can also be excited by radiation in any of the low-lying absorption bands[5] of the Mn^{2+} ion. Detection was provided by an E.M.I. 9558-B photomultiplier (S-20 response). The accuracy of the measurements of the wavelength maximum was estimated to be ~ 20 Å at low temperatures and decreased with increasing temperature (i.e., decreasing intensity). The linewidth was substantially independent of temperature except in the region of the fluorescence change and was approximately 500 Å wide.

Flash excitation for the lifetime investigations was provided by a General Radio type 1531-A Strobotac. The lifetime was determined from an oscilloscope trace of the photomultiplier which monitored the fluorescent decay.

The procedure for the measurements began with the cooling of the sample by placing liquid helium in the coolant reservoir of the Dewar. After the coolant had boiled away, the temperatures of both the post and the attached sample would rise. The thermal mass of the system provided a sufficiently slow rate of warming for measurements to be recorded.

RESULTS

In Figs. 1, 2, and 3, the various fluorescent properties of MnF_2 and $RbMnF_3$ are shown. We emphasize these particular results because the brighter fluorescences and greater crystal perfection result in more accurate measurements over a wider temperature range. Both materials show changes in fluorescent properties well below the Néel temperature. The data for MnF_2 show additional changes in the region of the magnetic ordering temperature (~ 67°K). Small changes are also found in the data for $RbMnF_3$.

In Figs. 4, 5, and 6, the fluorescent properties of $NaMnF_3$, $RbMnF_3$, and $CsMnF_3$ are shown as a function of temperatue and the known Néel temperatures[6] are indicated. Again, the fluorescent properties change at temperatures well below, as well as at, the Néel temperatures.

In certain of the data, the profiles near the region of the lower temperature transitions have the appearance of being composed of two separate fluorescent processes. The time-constant data provide strong support for this hypothesis. A separate determination of the two decay constants can be made for MnF_2 and $RbMnF_3$ in the region of T_H. This can be accomplished because of

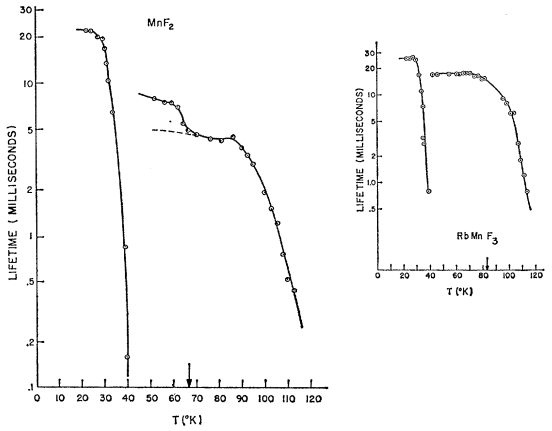

FIG. 3. The fluorescence lifetime of MnF_2 and $RbMnF_3$ as a function of temperature. The Néel temperatures are indicated by arrows.

[5] J. W. Stout, J. Chem. Phys. **31**, 709 (1959).

[6] V. L. Moruzzi and D. T. Teaney, Bull. Am. Phys. Soc. **9**, 225 (1964).

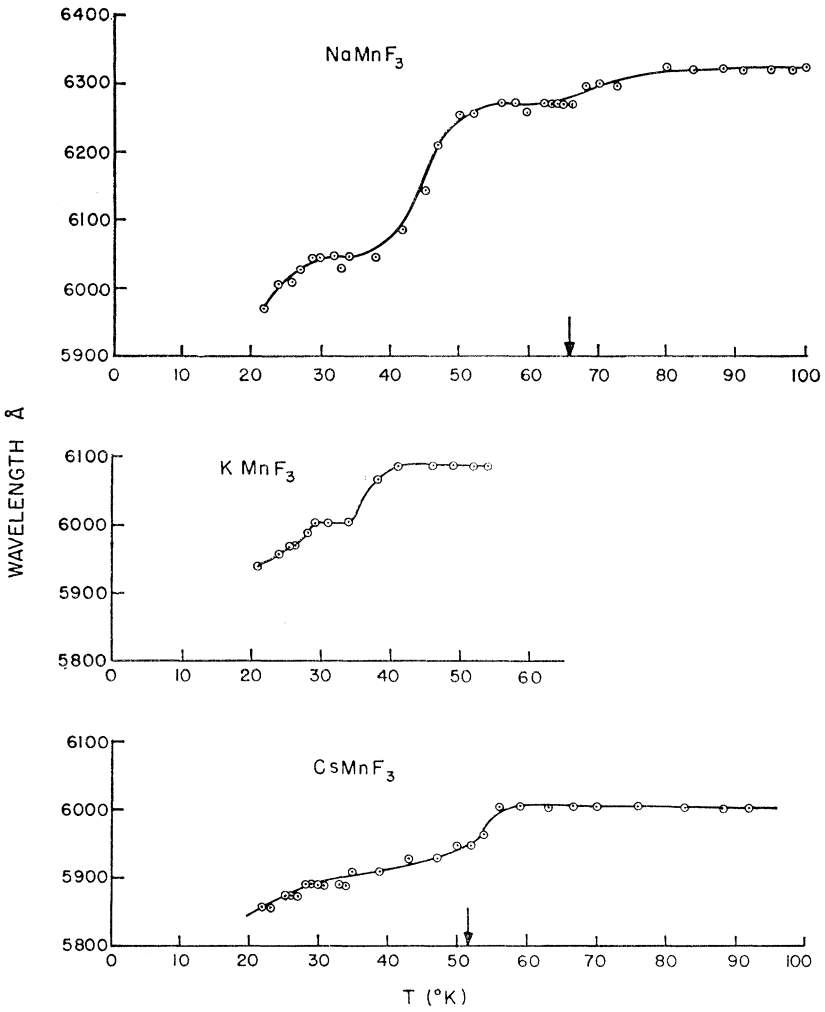

FIG. 4. The maximum wavelength of the fluorescence profiles of $NaMnF_3$, $KMnF_3$, and $CsMnF_3$ as a function of temperature. The Néel temperatures are indicated by arrows.

the wide separation of the $T>T_H$ and $T<T_H$ wavelengths. The anomalous lifetime behavior of the fluorescences of the Na and Cs salts may be due to the inability to separate lifetimes of the two fluorescent components with the present arrangement. In these cases, only an "average" lifetime could be measured.

Changes occur at the Néel temperature in at least one of the fluorescence properties. Further, the magnitude of the wavelength changes appears to increase with decreasing Néel temperature, i.e., $RbMnF_3$ ($T_N=82°K$) $\Delta E\sim 50\ cm^{-1}$, MnF_2 ($T_N=67°K$) $\Delta E\sim 130\ cm^{-1}$, $NaMnF_3$ ($T_N=66°K$) $\Delta E\sim 130\ cm^{-1}$, and $CsMnF_3$ ($T_N=51°K$) $\Delta E\sim 200\ cm^{-1}$.

The fluorescence alterations at $T_H\approx\frac{1}{2}T_N$ (Néel) require special comment because of the very strong functional dependence on temperature. These changes are not related to any crystal cooperative phenomena, such as structure changes. Any simple mechanism for these alterations, which does not involve cooperative phenomena, would have an exponential or "activation"-type temperature dependence. The intensity and the related lifetime mesaurements both reveal a much stronger dependence. (The functional relationship of the fluorescence wavelength maxima will not be significant if two fluorescence transitions are present.) The next section discusses how this strong dependence is attributed to a coupling of the lattice distortion, surrounding the excited Mn^{2+} ion and the surrounding ordered lattice.

It is interesting to note that $RbMnF_3$ and MnF_2 reach a common, low-temperature asymptotic wavelength of 5820 Å. There is an indication that, for $CsMnF_3$, approximately the same value will be reached at lower temperatures than were available.

THEORY

As previously stated, it is believed that the fluorescence alterations are due to an interaction between local lattice distortion and magnetic alignment of the Mn^{2+} ion. The magnetic nature is indicated because the effect is observed only in materials which become

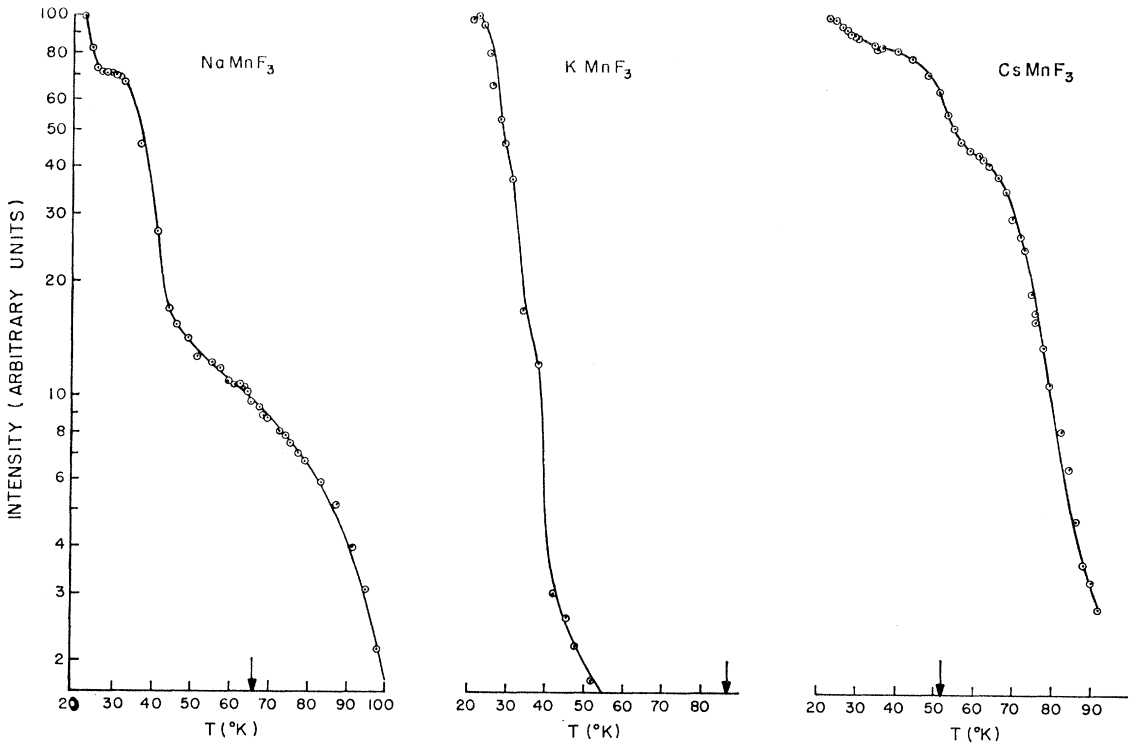

FIG. 5. The relative intensity of the fluorescence profiles of $NaMnF_3$, $KMnF_3$, and $CsMnF_3$ as a function of temperature. The Néel temperatures are indicated by arrows.

magnetically ordered. The importance of the lattice is evident in the fact that the shifts in fluorescent energy are typically of the order of 10^3 cm^{-1}, whereas the magnetic energies are typically 50 cm^{-1}. Stokes' shifts with energies larger than 10^3 cm^{-1} have been reported in these materials.[7] It is believed that lattice distortion caused by magnetoelastic effects subtracts from the normal Stokes' shift, causing the fluorescent alterations observed.

This mechanism is illustrated in Fig. 7. The figure is basically a configurational coordinate picture for various degrees of magnetic alignment. A configurational co-

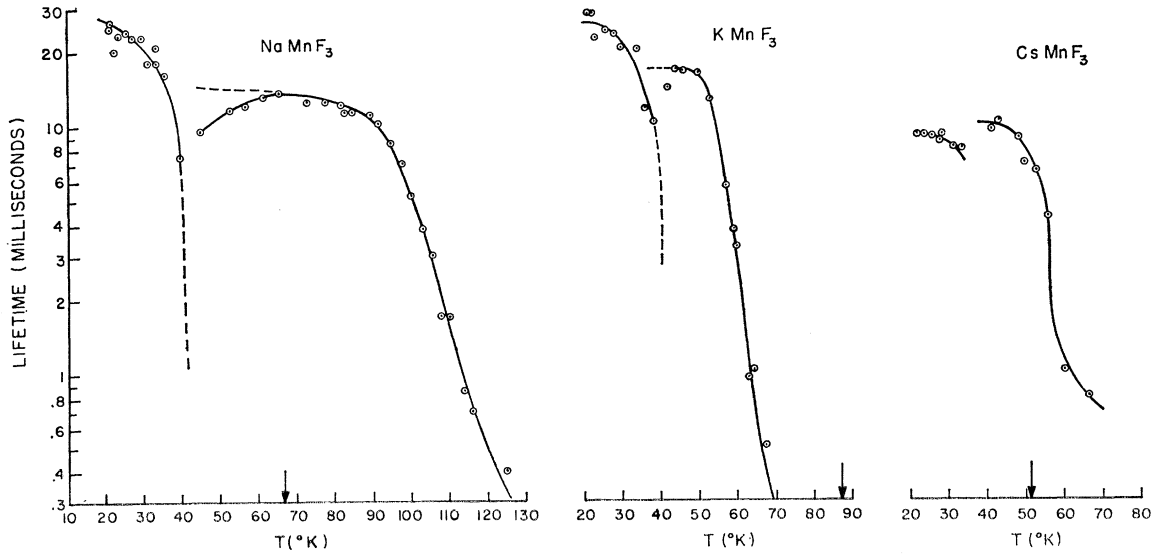

FIG. 6. The fluorescence lifetime of $NaMnF_3$, $KMnF_3$, and $CsMnF_3$ as a function of temperature. The Néel temperatures are indicated by arrows.

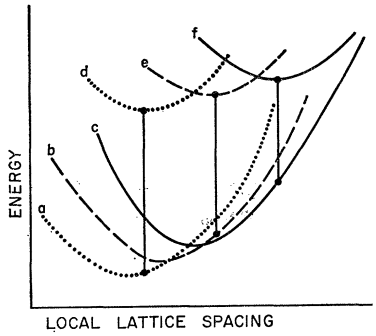

FIG. 7. Configurational coordinate curves for concentrated Mn salts. Curves *a*, *b*, and *c* represent various degrees of magnetic alignment of the optical ground state. Curve *a* is the most strongly aligned, *c* is randomly aligned. Curves *d*, *e*, and *f* represent the long-lived fluorescent state for similar degrees of magnetic alignment. A vibrational and magnetic Condon effect is assumed, and fluorescent emission occurs from $a \leftarrow d$, $b \leftarrow e$, and $c \leftarrow f$.

ordinate analysis has been successfully applied to high-temperature luminescence of divalent manganese by Klick and Schulman.[7] The validity of the approach has been investigated by Williams and Hebb[8] and by Lax.[9] In the figure, curves *a*, *b*, and *c* represent the ground state of the ion with respect to optical transitions. The differences in energy (exaggerated for emphasis in this figure) arise from the degrees of alignment of the ion magnetic moment in the internal magnetic field. Curve *a* is the most strongly aligned, and curve *c* is randomly aligned. It is not expected that the degree of alignment is quantized in such a concentrated system. Curves *a*, *b*, and *c* are part of a continuum distribution and are separated only for descriptive purposes. The upper set of curves *d*, *e*, and *f* represent the excited fluorescent level for various degrees of excited-state magnetic alignment. Curve *d* is the most strongly aligned and *f* is randomly aligned. Again, these curves are not quantized in magnetic alignment.

The displacement coordinate is a generalized coordinate such as that described by Lax,[9] but it is physically related to a local lattice displacement along the "*c*" axis. This coordinate is, then, a measure of the spacing between the Mn and F near-neighbor ions. The minima of the optically excited-state curves (*d*, *e*, and *f*) are placed on the locally dilated side of the ground-state minima. This is because the degree of covalency in these Mn compounds is expected to be large, as was the case in similar Ni compounds as calculated by Sugano and Shulman,[10] The excited fluorescent state in $Mn(t_{2g}^4 e_g)$ has smaller electron density between the Mn and F nuclei than the ground state ($t_{2g}^3 e_g^2$). The reduction of charge which shields the repulsion of the nuclei should cause local dilation in the excited state.

The equilibrium spacing of the configurational coordinate is seen to decrease with increasing magnetic alignment. For the optical ground state, curves *a*, *b*, and *c*, this agrees with measurements of the "*c*"-axis contraction by Gibbons.[11] In general, one expects the antiferromagnetic alignment (opposite electronic spin on neighboring ions) to allow closer ionic separations. This magnetoelastic effect has been drawn so as to be greater for the excited state than for the ground state. The ground state is an *S* state and therefore one expects it to be less susceptible to distortion. The configuration-coordinate effective-spring constant for the ground state was found by Klick and Schulman[7] to be much larger than that of the excited state, which also implies a greater magnetoelastic effect for the excited fluorescent ion. This difference in compressibility is reflected in the larger curvature for the ground-state parabolas in Fig. 7.

To determine the energy of fluorescent emission, we assume a magnetic as well as a vibrational Condon principle. The energy of the photon is determined by the energy of the transition to the lower electronic configuration assuming no change in either lattice distortion or spin alignment. The final ground state is achieved by the simultaneous or subsequent emission of phonons and spin waves. In terms of Fig. 7, this means that optical emission energy is that from $d \rightarrow a$, $e \rightarrow b$, and $f \rightarrow c$. The fluorescence is therefore determined by the degree of magnetic alignment of the long-lived excited fluorescent state. The absorption spectra would, however, be determined by the alignment of the ground state.

The magnetic orientation of the excited fluorescent state is determined by the degree of thermal activation of a magnetic virtual local mode. The nature of this activation and of the condensation of the local mode is discussed in the next section. For purposes of understanding the fluorescence, we assume that at lowest temperatures $T<T_H$ this mode is not thermally activated and the fluorescent ion is strongly aligned (i.e., in level *d*). The fluorescence in this temperature range is characterized by the transition $d \rightarrow a$. At somewhat higher temperatures $T_H<T<T_N$ the local mode is thermally activated, which reduces the degree of alignment of the fluorescent ion (i.e., in level *e*). The optical transition is then $e \rightarrow b$. Some degree of alignment is maintained as long as an internal field exists. At $T>T_N$ no internal field is present and the fluorescent ion is randomly aligned (i.e., in level *f*). The optical transition at these temperatures is then $f \rightarrow c$.

At these temperatures the vibrational levels would not be thermally activated and the vibrational wave function in the optically excited state would be Gaussian,

[7] C. C. Klick and J. H. Schulman, J. Opt. Soc. Am. **42**, 910 (1952).
[8] F. E. Williams and M. H. Hebb, Phys. Rev. **84**, 1181 (1951).
[9] M. Lax, J. Chem. Phys. **20**, 1752 (1952).
[10] S. Sugano and R. G. Shulman, Phys. Rev. **130**, 517 (1963). K. Knox, R. G. Shulman, and S. Sugano, Phys, Rev. **130**, 512 (1963). R. G. Shulman and S. Sugano, Phys. Rev. **130**, 506 (1963).
[11] D. F. Gibbons, Phys. Rev. **115**, 1194 (1959).

centered about the minima in the potential curves d, e, or f. This wave function would peak over the potential minima, making emission from directly above the potential minimum the most probable result. The fluorescent intensity maximum plotted in Figs. 1 and 4 would correspond to the lines drawn in Fig. 7. The independence of the linewidth on temperature also indicates that the vibrational levels are not thermally activated and the linewidth is determined only by the spread in the zero-point wave functions.

Since the magnetoelastic effect is assumed larger for the optically excited levels, the shift due to magnetic alignment subtracts from the usual Stokes' shift. This causes the energy of the optical transition $d \rightarrow a$ (i.e., $T<T_H$) to be greatest and $f \rightarrow c$ ($T>T_N$) to be smallest. The rapidity of the shift in the energy of the fluorescence at T_H is explained by the condensation phenomenon associated with the local mode. The shift at T_N is expected to follow the magnetization, as is the case experimentally.

The data on fluorescence lifetime can also be explained using the configurational coordinate model. Since the vibrational levels are not thermally activated, one would expect the main relaxation mechanism to be nonradiative tunneling as described by Huang and Rhys,[12] and Kubo.[13] This tunneling rate is determined by the overlap of the vibrational wave functions between the upper and lower set of levels of the same energy. This overlap would be a strong function of the horizontal distance from the minima of the upper set of curves to the lower curves. That is the overlap of the zero-point wave function of the excited state centered at the potential minima, and the highly energetic vibration of the optical ground state with large density at the classical turning point.[12] This overlap would grow progressively smaller from level d to f. The strongly aligned level d would have the longest lifetime, level f the shortest. The intensity data follow from the lifetime curves when the lifetime is primarily due to nonradiative interactions such as tunneling.

The rapid decrease in lifetime of the high-frequency fluorescence, as T approaches T_H from below, can be understood when it is realized that at $T_H<T<T_N$ the ground state is more strongly aligned than the excited state. The alignment of the ground state follows the magnetization. Only the existence of the smaller total spin and weaker superexchange parameter (i.e., the defect) allows the optically excited state to be less strongly aligned at temperatures below T_N. For $T_H<T<T_N$, the excitation then occurs from $a \rightarrow d$ and it requires a time of the order of a spin-spin relaxation for the excited level to reduce its alignment (i.e., $d \rightarrow e$). As $T \rightarrow T_H$, then, the relaxation time of the high-frequency emission ($d \rightarrow a$) approaches the spin-spin relaxation time.

[12] K. Huang and A. Rhys, Proc. Roy. Soc. (London) **A204**, 406 (1950).
[13] R. Kubo, Phys. Rev. **86**, 929 (1952).

THE CONDENSATION MECHANISM

At the position of the optically excited site there exists a local spin defect with lower local magnetic energy than at other (unexcited) sites. In such a case, a local mode of the virtual type exists. It is called virtual because its energy lies within the antiferromagnetic spin-wave quasicontinuum and it interacts very strongly with the continuum spin waves. The energy of this local mode is determined by magnetic parameters at the defect site, such as the defect spin and the exchange energy between the defect and its neighbors. By altering the exchange energy the local displacements provide a feedback mechanism to the magnetic system, altering the local mode and, therefore, the magnetic alignment. The direction of this cooperative effect is to reduce the energy of the virtual local mode as it becomes thermally activated. This results in further thermal activation, etc. With *decreasing* temperature, on the other hand, the energy of the local mode suddenly increases as thermal deactivation occurs, giving rise to the condensation of the local mode.

Virtual local modes in phonon spectra and in ferromagnetic systems have been investigated extensively.[14–16] One expects the results to be similar for antiferromagnetic spin waves. Because of line broadening by interaction with the continuum modes, a better description can be derived by assuming that the virtual local mode is made up of a superposition of continuum modes. The amplitude in the phonon case, or the alignment in the magnetic case, is primarily determined by the amplitude of a narrow band of phonons, or spin waves, with energy centered about the energy of the "would-be" local mode. The coupling of continuum modes to the defect site has been plotted in Fig. 2 of Dauber and Elliot.[15] Because of the large number of continuum modes which make up the local mode, one can apply statistical averages to determine the degree of thermal activation. These spin-wave modes are expected to reach thermal equilibrium in times of the order of spin-spin relaxation times. Spin-spin relaxation times are much shorter than the lifetime of the fluorescent state, and the emission can be thought of as occurring from a thermally equilibrated state.

The magnetoelastic effect responsible for the shift of levels in Fig. 7 can be simply treated by letting

$$J^0=J_1-J_2(x/a)\,, \tag{1}$$

where J^0 is the total superexchange constant between the excited ion and its magnetic neighbors, J_1 is the constant part, J_2 is the coefficient of the linear variation with displacement, and x/a is a dimensionless displacement (i.e., $a \rightarrow b$ or $d \rightarrow e$). The vibrational Hamiltonian in the vibronic-state approximation then

[14] R. Brout and W. Visscker, Phys. Rev. Letters **9**, 54 (1962).
[15] P. G. Dauber and R. J. Elliot, Proc. Roy. Soc. (London) **A273**, 222 (1963).
[16] J. Callaway, Phys. Rev. **132**, 2003 (1963).

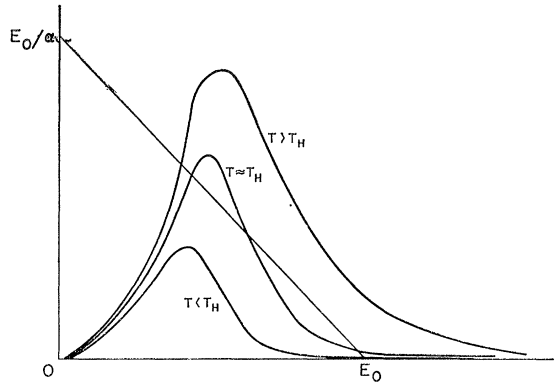

FIG. 8. The solution $\bar{E}$ of the Eq. (7) is given by the intersection of the line $(E_0-\bar{E})/\alpha$ with $n(\bar{E})=\bar{E}^2(e^{\bar{E}/KT}-1)^{-1}$. For $T<T_H$ the solution is very close to E_0. For $T>T_H$ the solution is very much less than E_0. The change is discontinuous with some possibility of unstable solutions at $T\approx T_H$.

becomes

$$\mathcal{H}_{\text{vib}}+\mathcal{H}_{\text{int}}=(P^2/2M)+\tfrac{1}{2}Kx^2-\sum_j J_2\mathbf{S}^0\cdot\mathbf{S}^j\frac{x}{a}, \quad (2)$$

where P and M are the momentum and mass associated with the vibronic state, K is its spring constant, $\mathbf{S}^0$ is the spin of the excited ion, $\mathbf{S}^j$ is the spin at all other sites of the crystals, and the sum is over near neighbors j. By completing the square, Eq. (2) can be written as

$$\mathcal{H}_{\text{vib}}+H_{\text{int}}=(P^2/2M)+\tfrac{1}{2}K(x-\langle x\rangle)^2+\text{const}, \quad (3)$$

where

$$\langle x\rangle=\frac{mJ_2\langle s_z{}^j\rangle}{Ka}\langle S_z{}^0\rangle=\frac{mJ_2S^jS^0}{KaN}[1-\sum_{\Delta E} n(E)], \quad (4)$$

where m is the number of near neighbors, $n(E)$ is the spin-wave occupation with energy E, and ΔE signifies the spread over those states which make up the local mode. The minima of the parabolas in Fig. 6 are at $\langle x\rangle$, where $\langle x\rangle$ is determined by the degree of alignment $\langle S_z{}^0\rangle$, which in turn is determined by the degree of thermal activation $n(\bar{E})$.

The sum in Eq. (4) can be limited to the states of the virtual local mode since these states provide most of the coupling to the defect site. The average values of $\mathbf{S}^0$ and $\mathbf{S}^j$ can be taken because the sum consists of many spin-wave states even though they are all close in energy. The net thermal averages of $\mathbf{S}^j$ and $\mathbf{S}^0$ are then $\langle S_z{}^j\rangle$ and $\langle S_z{}^0\rangle$. The $\langle S_z{}^j\rangle$ are more aligned below the Néel point, as they are coupled to higher energy spin waves. Since the local modes are close in energy, we will set

$$\sum_{\Delta E} n(E)=\Delta n n(\bar{E}). \quad (5)$$

The defect in energy about the defect site is

$$\epsilon=(J^0S^0-J^jS^j)S^j. \quad (6)$$

When this parameter is negative the modes are virtual. Making use of Eqs. (1), (5), and (6), this becomes

$$\epsilon=-|\epsilon_0|-|\epsilon_1|n(\bar{E}). \quad (7)$$

The energy $\bar{E}$ of the local mode should decrease monotonically with decreasing ϵ. This is shown to be the case for phonons by Dauber and Elliot.[15] To a first approximation we will assume

$$\bar{E}(T)=E_0+\beta\epsilon, \quad (8)$$

and using Eq. (7),

$$\bar{E}(T)=E_0-\alpha n(\bar{E}). \quad (9)$$

A system described by Eq. (9)[17] will undergo a discontinuous change with temperature as shown by the graphical solution in Fig. 8. We assume that the density of spin-wave states coupled to the local mode is not too different from the actual spin-wave density at the energy $\bar{E}$. The factor $n(\bar{E})$ is then

$$n(\bar{E})=\bar{E}^2[\exp(\bar{E}/kT)-1)^{-1}. \quad (10)$$

The solutions of Eq. (9) are then the intersection of $E_0/\alpha-\bar{E}/\alpha$ and $n(\bar{E})$. At very low temperatures, $T<T_H$, the energy of the spin waves making up the local mode is $\bar{E}\approx E_0$. The local mode is not thermally activated as $kT<E_0$. At high temperatures $T>T_H$, $\bar{E}<kT$, and the local mode will be thermally activated. Except when α becomes vanishingly small, the change in the solution of $\bar{E}$ is discontinuous. The discontinuous solution is possible even when the linear approximation Eq. (8) is not valid. This can be seen from Fig. 8 by adding curvature to the line $E_0/\alpha-E/\alpha$. A discontinuous change in $\bar{E}$ with T causes a discontinuous change in $n(\bar{E})$. This in turn alters $\langle x\rangle$ [Eq. (4)] and the fluorescent emission discontinuously.

It should be pointed out that Eqs. (8) and (10) require justification from local-mode theory applied to antiferromagnetic systems. At present, they may be justified by analogy to the local-mode analysis for phonon[14,15] and ferromagnetic[16] systems. The antiferromagnetic case is considerably more difficult. However, the basic transition mechanism described is not dependent on the exact forms for Eqs. (8) and (10), but should be possible for monotonic decrease in $\bar{E}$ with ϵ and almost any reasonable form of $n(\bar{E})$.

CONCLUSION

Changes in the fluorescences of MnF_2 and the alkali manganese trifluorides are observed as a function of temperature. Small changes are observed in the vicinity of the Néel temperature. Larger and more strongly temperature-dependent alterations are observed at roughly one-half the Néel temperature.

[17] An equation similar to Eq. (9) has been used by D. Adler and J. Feinleib, Phys. Rev. Letters 12, 700 (1964), to describe the semiconductor-to-metal transition in V_2O_3.

The fluorescent behavior of concentrated Mn salts can be explained within the framework of the vibronic-state model. The magnetic effects alter the Stokes' shift by a magnetoelastic effect. The very abrupt transition at T_H can be explained by assuming that a magnetic local mode is strongly affected by lattice distortions. There exists a cooperative effect between local magnetic alignment and local lattice distortion which causes a condensation in the thermal excitation of the magnetic local mode.

ACKNOWLEDGMENTS

We are pleased to acknowledge many enlightening discussions with Dr. R. Newman, Dr. J. Shane, Dr. M. Klein, and Dr. D. McMahon concerning the results described in this paper.

PHYSICAL REVIEW VOLUME 139, NUMBER 3A 2 AUGUST 1965

Anisotropic Oxygen Polarizability and the Lorentz Correction in $BaTiO_3$†

W. N. LAWLESS*

Interdisciplinary Materials Research Center, Rensselaer Polytechnic Institute, Troy, New York

(Received 22 June 1964; revised manuscript received 29 March 1965)

The temperature dependence of the electronic polarizabilities of the ions in $BaTiO_3$ is incorporated in the Slater-Devonshire theory under the assumption that the dominant contribution arises from the O_a electronic polarizability due to the large Ti-O_a overlap along the polar axis. The temperature dependence of the O_a polarizability as determined from optical data is parameterized in the spontaneous polarization, and a free-energy function for the clamped crystal is derived and compared with the (adjusted) experimental free energy. An internal check on this comparison yields $(dB/dT)=5.63\times10^{-15}$ cgs units, compared with the experimental value 4.5×10^{-15} (B is the fourth-order coefficient in the free energy). A minimum-internal-energy calculation is performed for the clamped crystal polarized along [001], corresponding to the tetragonal phase. This calculation illustrates the role of the O_a polarizability in limiting the spontaneous polarization: Using the O_a polarizability anisotropy data, a spontaneous polarization of 59 600 esu is obtained; if the isotropic oxygen polarizability in the cubic phase is used, 667 000 esu. Similar calculations are performed for the clamped crystal polarized along [011] and [111], corresponding to the orthorhombic and rhombohedral phases, respectively. The O_a polarizability anisotropy data are used, and for the [011] calculation a spontaneous polarization of 33 300 esu is obtained. It is found that the Lorentz correction for the clamped crystal corresponding to a [111] polar axis is not large enough to support a spontaneous polarization, but that a shear of the unit cell of about 27′ is required to stabilize a spontaneous polarization along this axis.

INTRODUCTION

THE various molecular theories of ferroelectricity in $BaTiO_3$ deal, quantitatively or qualitatively, with the Lorentz internal fields in the perovskite lattice and the energy states of the Ti^{4+} ion or the TiO_6 octahedra; these theories are reviewed in the book by Jona and Shirane.[1] In particular, the theory due to Slater[2] considers a displaceable Ti ion in a clamped (zero-strain) $BaTiO_3$ unit cell and from the classical partition function an expression for the local field at the Ti site is derived. This local field is then used in an analysis of the inner fields including the electronic polarizations, and this analysis permits the external field to be written as a power series in the total polarization; by integration, a free-energy expression for the clamped crystal is obtained. The salient features of Slater's theory are the enhanced dipole coupling between the Ti and O_a ions along the polar axis (see Fig. 1 which is a schematic drawing of the $BaTiO_3$ unit cell) and the relatively small role of the Ba and O_b ions in the clamped-crystal approximation.

The phenomenological theory of Devonshire[3,4] consists of expanding the free energy in a power series of polarizations and strains, or polarizations and stresses, and assuming that this single function applies to the paraelectric and ferroelectric phases. By examining the behavior of certain of the expansion coefficients, the behavior of others can be deduced, and in this fashion Devonshire has accounted for the dielectric, elastic, and piezoelectric properties of $BaTiO_3$ through three phase changes. These phenomenological free-energy expansions provide the basis for treating experimental data, and, in particular, the free-energy function for the actual crystal (zero stress) can be adjusted to a free-energy function for the clamped crystal for comparison with the molecular-model calculations.

† Research sponsored by a National Aeronautics and Space Administration research grant; from a portion of a thesis presented in partial fulfillment of the requirements for the Ph.D. degree in Physics, Rensselaer Polytechnic Institute, Troy, New York.

* Currently a postdoctoral fellow at the Laboratorium für Festkörperphysik, ETH, Zürich.

[1] F. Jona and G. Shirane, *Ferroelectric Crystals* (The Macmillan Company, New York, 1962), Chap. IV.

[2] J. C. Slater, Phys. Rev. **78**, 748 (1950).

[3] A. F. Devonshire, Phil. Mag. **40**, 1040 (1949).

[4] A. F. Devonshire, Phil. Mag. **42**, 1065 (1951).